

TREND towards more energy-efficient optical networks

Original

TREND towards more energy-efficient optical networks / E., Le Rouzic; Bonetto, Edoardo; Chiaraviglio, Luca; F., Giroire; F., Idzikowski; F., Jimenez; C., Lange; J., Montalvo; F., Musumeci; I., Tahiri; A., Valenti; W., Van Heddeghem; Y., Yabin; Bianco, Andrea; A:pattavina,. - STAMPA. - (2013), pp. 211-216. (Optical Network Design and Modelling 2013 Brest, France April 2013).

Availability:

This version is available at: 11583/2606214 since:

Publisher:

IEEE - INST ELECTRICAL ELECTRONICS ENGINEERS INC

Published

DOI:

Terms of use:

This article is made available under terms and conditions as specified in the corresponding bibliographic description in the repository

Publisher copyright

IEEE postprint/Author's Accepted Manuscript

©2013 IEEE. Personal use of this material is permitted. Permission from IEEE must be obtained for all other uses, in any current or future media, including reprinting/republishing this material for advertising or promotional purposes, creating new collecting works, for resale or lists, or reuse of any copyrighted component of this work in other works.

(Article begins on next page)

Polarization-related Statistics of Raman Cross-talk in Single-mode Optical Fibers

Mattia Cantono, *Student Member, IEEE*, Vittorio Curri, *Member, IEEE*, Antonio Mecozzi, *Fellow, OSA, Fellow, IEEE* and Roberto Gaudino, *Member, IEEE*,

Abstract—We present a novel comprehensive theory for the pump-to-probe interactions caused by the stimulated Raman scattering (SRS) in glass optical fibers. The developed theory applies to both the Raman gain with the un-depleted pump assumption and to the maximum loss induced by the Raman cross-talk (RXT loss). The latter is an effect that is the limiting propagation impairment in passive optical networks (PON).

The main novelty of the paper is a rigorous mathematical analysis describing the interaction of SRS with the polarization evolution due to polarization mode dispersion (PMD). The Raman gain (or the RXT loss) is modeled as a random process for which a comprehensive theory is developed, giving for the first time to our best knowledge, an exact closed form expression for the mean and variance of the gain (or depletion) and a computationally efficient algorithm to numerically derive the gain probability density function.

The developed theory is validated by the comparison with Monte Carlo analyses based on the waveplate model for the optical fiber. The validation showed excellent agreement confirming the validity of the developed theory.

As an example of application, we used our theoretical results to analyze next generation PON (NG-PON2) architectures, confirming that, in this scenario, RXT loss may be a limiting propagation effect.

Index Terms—Optical Communications, SRS, Raman Effect, Raman Crosstalk

I. INTRODUCTION

THE Raman effect was first observed in 1928 [1], then was formalized as stimulated Raman scattering (SRS) in 1962 [2], and, in optical communications, was initially observed in silica core fibers in 1972 [3], [4]. SRS enables, in every spectral window, power transfer from every higher frequency – the *pump* – to every lower frequency – the *probe* – with some losses as mechanical energy – *phonons*. The spectral shape of the normalized Raman efficiency in SiO₂ [4], [5], [6] is shown in Fig. 1 as a function of the *pump-to-probe* frequency offset (Δf). It can be observed that it grows roughly linearly with Δf up to the maximum at $\Delta f \approx 13$ THz ($\Delta\lambda \approx 100$ nm), then, after a minor notch, it quickly decreases for $\Delta f > 15$ THz ($\Delta\lambda \approx 120$ nm).

Since all single-mode fibers are mainly made of SiO₂, they are all affected by the SRS according to the spectral shape shown in Fig. 1, while its intensity grows along the same trends as the Kerr effect (i.e. the intensity increases for larger

nonlinear refractive index n_2 and smaller effective area A_{eff}). SRS is independent on the propagation direction, so it couples both co- and counter-propagating signals.

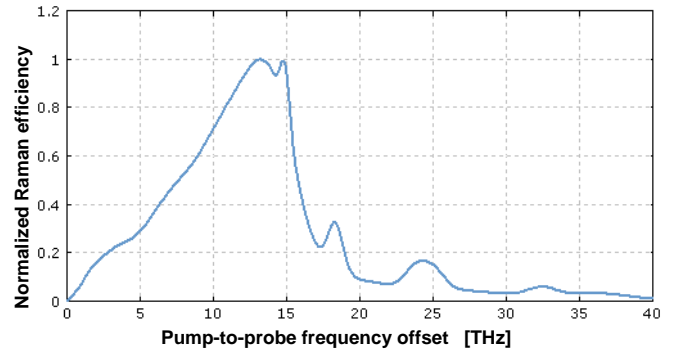


Figure 1. Raman efficiency in SiO₂ vs. the pump-to-probe spectral offset.

Since the beginning of optical communications, SRS was considered as a resource, being a physical mechanism useful for the implementation of optical amplifiers, first outside the C-band [7], [8], [9], then, already in 1985 [10], in the C-band. Even if the standard technology for optical amplification is the Erbium-doped fiber amplification (EDFA), the investigation on Raman amplifications (RA) has continued, as shown, for instance, in [11]–[15], [16], [17].

Besides enabling optical amplification, SRS excites interactions between the transmitted channels, resulting in a spectral tilting of the channel comb implying an extra loss on higher frequency channels that grows up to the one at the highest frequency that only transfers power to the other channels without receiving any gain. This effect is commonly called Raman cross-talk (RXT) and it is typically quantified using the RXT loss experienced by the highest frequency channel. From Fig. 1, we deduce that the RXT intensity depends on the overall optical bandwidth occupied by the channels compared to the SRS bandwidth, roughly 15 THz.

Focusing on high-capacity back-bone links, supposing to operate on the C-band that extends on 5 THz, the intensity of SRS is limited at about 25% of its maximum value. The resulting effect is a spectral tilting of the channel comb spectrum that, on state-of-the-art transmission bandwidth, can be compensated for. In these system scenarios, RXT will possibly become a major issue in next-generation long-haul links using also the S- and L-band, and in transmission over multi-core fibers.

On the contrary, in some recent implementation of passive

M. Cantono, R. Gaudino and V. Curri are with Dipartimento di Elettronica e Telecomunicazioni, Politecnico di Torino, Italy (email: mattia.cantono@polito.it)

A. Mecozzi is with the Department of Physical and Chemical Sciences, University of L'Aquila, Italy (e-mail: antonio.mecozzi@univaq.it)

optical networks (PON), RXT is already a limiting issue, as analyzed in [18]–[21], since different services are placed on different wavelengths in both the C- and L-band simultaneously, and may thus have a spectral separation close to the Raman peak. In particular, in NG-PON2 [22], the activation of TWDM-PON channels at 1600 nm may strongly deplete the already operating GPON channel at 1500 nm, possibly causing its out-of-service [23], [24].

SRS depends on the evolution with propagation of the states of polarization (SOP) of the signals involved in the process, as it is mainly effective among signals locally characterized by the same SOP [25]. Therefore, any variation of signal SOPs with time and distance makes the RXT vary consequentially. Since the variation of SOPs is a random process, the RXT loss is stochastic as well, and its characterization is required in order to estimate the probability of out-of-service they may induce [23], [24]. It is well known that in optical fibers, the main physical effects causing change of SOPs are the birefringence and the phenomenon generated by its random variation, i.e., the polarization mode dispersion (PMD). The PMD causes the SOPs to vary randomly versus the propagation distance, depending on the launched SOPs and on the system characteristics [26], [27]. Moreover, as the PMD is mostly induced by mechanical stresses suffered by the fiber cable, its random evolution in the fiber varies with time.

As a consequence, in general, the RXT loss is a random process, depending on the system characteristics and on the input SOPs of the involved signals and varying with time.

The effects of PMD on SRS have been extensively studied in the context of RA both experimentally [28]–[31] and theoretically [32], [33]. Note that results for RA with the *undepleted pump assumption* can be reused for the context of RXT with the *un-filled probe assumption* just swapping RA gain with RXT loss. In [32], [33], theoretical analyses for the statistics of Raman gain are presented, even if limited to specific scenarios. In particular, in [33], a complete analysis of the statistics of Raman gain for random input SOPs is carried out, and it is shown that the probability density function (PDF) of the Raman gain in that case is given by a log-normal, Gaussian in dB, distribution with known mean and variance. For the RXT-loss, such a result, among others, is confirmed in [23], [24]. In [33], the case of known input SOPs is not analyzed while it is done in [32]. In such a publication, the authors develop and present a set of differential equations, depending on input SOPs and fiber PMD, for the average and variance of the Raman gain, but closed-form solutions are not presented. Moreover, as far as the PDF of the Raman gain is concerned, in [32], the PDF of its value in dB units is shown to be Gaussian for link lengths much larger than the PMD diffusion-length L_d , given by [32]:

$$L_d = \frac{\pi}{8\delta_{PMD}^2 \Delta\omega^2}, \quad (1)$$

where δ_{PMD} is the fiber PMD coefficient expressed in ps/km^{1/2} and $\Delta\omega = 2\pi\Delta f$ is the pump-to-signal spectral separation in circular frequencies.

In modern fibers the PMD coefficient is typically $\delta_{PMD} \leq 0.04$ ps/km^{1/2}, and considering the worst-case spectral sep-

aration for RXT, i.e., $\Delta f \approx 13$ THz ($\Delta\lambda \approx 100$ nm), we obtain diffusion lengths of the order of tens of kilometers. Hence, in the PON environment, for which the distance does not exceed 40 km, the diffusion length is indeed comparable to the propagation distance and results presented in [32] cannot be used.

In this paper, in order to present a comprehensive analysis including the PON environment where RXT loss is indeed a limiting effect, we aim at being as general as possible. In particular, the main novelty of our paper is the provision of closed-form results for the average value and variance of the RA gain (or RXT loss) for the general scenario with given input SOPs, without any limitations to the length-to- L_d ratio. Moreover, we present for the first time to our best knowledge, a numerical method to exactly evaluate the PDF of the gain, again in the general case. In particular we show that the Raman gain is proportional to the integral of a cartesian component of a particle freely diffusing on a sphere. A one dimensional version of this problem, namely the integral of the component of a particle freely diffusing on a circle, has been solved, in the small noise limit, in a seminal paper by Foschini and Vannucci in the context of the analysis of the noise of an integrate and dump receiver with a local oscillator of finite linewidth [34]. Thanks to the obtained results, we are able to statistically fully characterize the RXT loss with the possibility to estimate the related outage probability in PONs [23], [24]. In addition, we also provide an analytical approximation able to give the PDF of the Raman gain for very small values of PMD. All theoretical results are validated by comparison with numerical results obtained through Monte Carlo simulations based on the waveplate model [35], [36] for the fiber.

This paper is organized as follows. Sec. II is devoted to presenting the main theoretical analysis. Here for the first time, to our best knowledge, the average value, the variance and the PDF of the Raman gain (or RXT loss) are theoretical derived for any general system scenarios. In Sec. III, theoretical results developed and presented in the previous section are compared with those obtained through Monte Carlo simulations-based on the waveplate model. Comparisons display excellent agreements, validating the developed theory. In Sec. IV, we apply the developed and validated results to the PON scenario, demonstrating that SRS is indeed the propagation limiting effect together with the fiber loss, in PON, in case of co-existence of GPON and TWDM-PON channels. Finally, we draw some conclusions.

II. THEORETICAL ANALYSIS

In the following, we study the pump-to-probe interaction enabled by the SRS between two co-propagating continuous wave (CW) optical fields with a spectral separation equal to $\Delta\omega$. We analyze only the time-independent SRS, thus focusing on the resulting variation on the average power of the involved wavelengths, while we ignore the (second-order) time-dependent effects that induces relative intensity noise power transfer [37]. The developed theory applies to two different situations:

- the pump-to-probe gain (i.e. the RA gain) under the

un-depleted pump assumption, as typically applicable in distributed Raman amplifiers.

- the probe-to-pump loss (i.e. the Raman crosstalk depletion) under the *un-filled* probe assumption, i.e., the assumption that the probe benefits of negligible gain, as typically applicable in recent NG-PON2 transmission scenarios, where SRS causes depletion of a (relative weak) optical signal acting as Raman pump for other (relatively stronger) signals at higher wavelengths [20], [21], [23], [38].

Let us define an index i to discriminate between the two aforementioned scenarios:

$$i = \begin{cases} p & \text{for RA gain} \\ s & \text{for RXT loss} \end{cases} \quad (2)$$

where p corresponds to the pump optical field (the upper frequency signal), and s the signal – the probe – optical field (the lower frequency optical signal). Starting from the well known theory for RA [33], and assuming that the RA gain or RXT loss becomes negligible when the signal and pump are orthogonally polarized [25], [32], we can consider the following equation, that gives either the SRS gain experienced by the signal due to the pump presence, as in any Raman amplification scenario, or the SRS induced depletion suffered by the pump signal, as in PON scenario, in dB units:

$$G_{\text{dB}}(L) = 10 \log_{10}(e) C_r(\Delta\omega) P_i(z=0) [L_{\text{eff},i} + \text{DOP}_i \int_0^L \eta(z) \exp(-\alpha_i z) dz], \quad (3)$$

where L is the length of the fiber, $C_r(\Delta\omega)$ is the polarization averaged Raman gain coefficient at distance $\Delta\omega$, $P_i(z=0)$ is the optical power at the input of the fiber of either the signal or the pump, α_i is the fiber loss at the pump or signal frequency, DOP_i is the degree of polarization of either the pump or signal optical fields, $L_{\text{eff},i}$ is the effective length of the fiber given by

$$L_{\text{eff},i} = \frac{1 - e^{-\alpha_i L}}{\alpha_i}, \quad (4)$$

whereas $\eta(z)$ is given by

$$\eta(z) = \hat{s}_s(z) \bullet \hat{s}_p(z), \quad (5)$$

i.e. the dot product between the Stokes vector representing the SOP of the signal and the pump at position z . Due to the presence of PMD, the term $\eta(z)$ is a stochastic process, since the SOP of the optical fields randomly evolve during the propagation along the fiber due to its random birefringence variation [27]. This being said, Eq. (3) is given by the sum of two terms, a deterministic term and a stochastic integral. Starting from Eq. (3) we want to compute its average value, variance and PDF as a function of the input states of polarization of the pump and signal, and the PMD coefficient of the fiber.

A. Average of $G_{\text{dB}}(L)$

We start rewriting Eq. (3) as

$$G_{\text{dB}} = K L_{\text{eff},i} + K \text{DOP}_i \int_0^L \eta(z) e^{-\alpha_i z} dz, \quad (6)$$

where $K = 10 \log_{10}(e) C_r(\Delta\omega) P_i(z=0)$. Taking the average of Eq. (6) yields

$$\langle G_{\text{dB}} \rangle = \left\langle K L_{\text{eff},i} + K \text{DOP}_i \int_0^L \eta(z) e^{-\alpha_i z} dz \right\rangle, \quad (7)$$

The average operator in the previous and following equations is to be interpreted as an ensemble average over all possible polarization stochastic evolution. Thus, it is NOT an average over time or distance, but an ensemble average over polarization states.

Using the properties of the average operator, ignoring the deterministic terms and considering the degree of polarization of the optical fields to be maintained during propagation we get

$$\langle G_{\text{dB}} \rangle = K L_{\text{eff},i} + K \text{DOP}_i \left\langle \int_0^L \eta(z) e^{-\alpha_i z} dz \right\rangle. \quad (8)$$

Exchanging the integral and the average operator we get

$$\langle G_{\text{dB}} \rangle = K L_{\text{eff},i} + K \text{DOP}_i \int_0^L \langle \eta(z) \rangle e^{-\alpha_i z} dz. \quad (9)$$

Appendix A provides the detailed calculation of the moments and the PDF of $\eta(z)$. In particular, it is shown that

$$\langle \eta(z) \rangle = \eta(0) \exp \left[-\frac{1}{3} \Delta\omega^2 \gamma z \right], \quad (10)$$

where γ is given by

$$\gamma = \frac{3\pi}{8} \delta_{\text{PMD}}^2, \quad (11)$$

and $\eta(0)$ is the dot product of the two input SOP.

Plugging Eq. (10) into Eq. (9) yields

$$\begin{aligned} \langle G_{\text{dB}} \rangle &= K L_{\text{eff},i} \\ &+ K \text{DOP}_i \int_0^L \eta(0) \exp \left[-\frac{1}{3} \Delta\omega^2 \gamma z - \alpha_i z \right] dz. \end{aligned} \quad (12)$$

The integral of Eq. (12) can be easily solved yielding to

$$\langle G_{\text{dB}} \rangle = K L_{\text{eff},i} + K \text{DOP}_i \eta(0) L_{\text{pol}}, \quad (13)$$

where L_{pol} is given by

$$L_{\text{pol}} = \frac{1 - \exp \left[-\alpha_i L - \frac{\gamma}{3} \Delta\omega^2 L \right]}{\alpha_i + \frac{\gamma}{3} \Delta\omega^2}. \quad (14)$$

Fig. 2 depicts Eq. (13) as a function of the PMD coefficient of the fiber δ_{PMD} and for three different input SOP configuration, namely co-polarized, 45° oriented and orthogonally polarized signals.

It can be noticed that for low δ_{PMD} the input SOP are maintained during propagation, therefore their dot product can be considered as independent from z and factorized from the integral of Eq. (3), yielding

$$\lim_{\delta_{\text{PMD}} \rightarrow 0} \langle G_{\text{dB}} \rangle = K L_{\text{eff},i} (1 + \text{DOP}_i \eta_0). \quad (15)$$

As δ_{PMD} increases, the two input SOP will not maintain their relative position. The more they are scrambled, and the more they will be uniformly distributed over the Poincaré sphere.

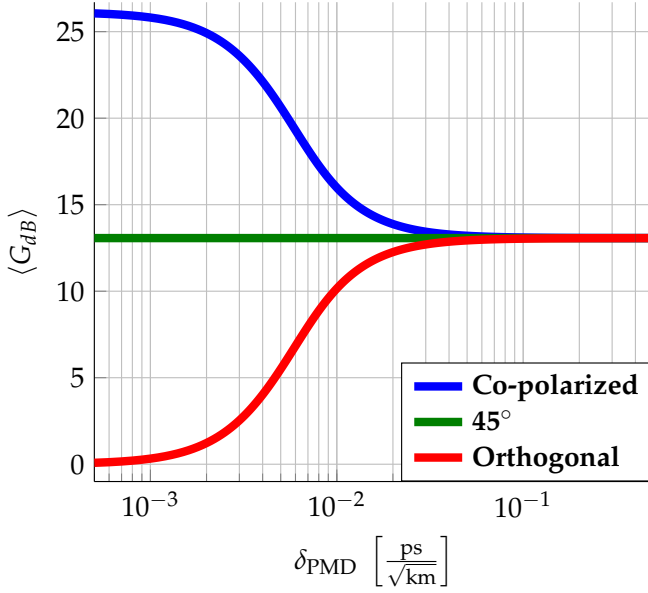


Figure 2. Average value of $G_{dB}(L)$ as a function of δ_{PMD} for a link length of 20 km, $K = 1$ dB/km, $\alpha_{i,dB} = 0.2$ dB/km and $DOP_i = 1$. Three different input SOP configurations are considered.

As δ_{PMD} is infinitely large, the two SOP can be considered uniformly distributed over the Poincaré sphere, and their dot product will be zero on average since the PDF of $\eta(z)$ will be uniformly distributed over the interval $[-1, +1]$, thus the same result of [33] is obtained.

$$\lim_{\delta_{PMD} \rightarrow \infty} \langle G_{dB} \rangle = KL_{eff,i}. \quad (16)$$

B. Variance of $G_{dB}(L)$

We now consider the variance of $G_{dB}(L)$ that is given by

$$\sigma_{dB}^2 = \langle G_{dB}^2 \rangle - \langle G_{dB} \rangle^2. \quad (17)$$

To compute the second order moment of G_{dB} we consider

$$\begin{aligned} \langle G_{dB}^2 \rangle &= K^2 L_{eff,i}^2 + 2K^2 DOP_i L_{eff,i} \eta(0) L_{pol} \\ &\quad + K^2 DOP_i^2 I_2(L), \end{aligned} \quad (18)$$

where the last term of the summation is given by

$$I_2(L) = \left\langle \left[\int_0^L \eta(z) e^{-\alpha_i z} dz \right]^2 \right\rangle. \quad (19)$$

Applying Fubini's theorem [39] we shall compute

$$I_2(L) = \int_0^L \int_0^L \langle \eta(z') \eta(z'') \rangle e^{-\alpha_i(z'+z'')} dz' dz''. \quad (20)$$

In order to compute the correlation $\langle \eta(z') \eta(z'') \rangle$ we start considering the case $z' \geq z''$ and the conditional expectation of $\eta(z')$ given $\eta(z'')$, i.e. [40]

$$\langle \eta(z') | \eta(z'') \rangle = \eta(z'') \exp \left[-\frac{1}{3} \Delta \omega^2 \gamma (z' - z'') \right]. \quad (21)$$

Knowing that $\langle \langle X | Y = y \rangle \rangle = \langle X \rangle$ [41], we can multiply both sides of Eq. (21) by $\eta(z'')$ and averaging with respect to all possible $\eta(z'')$, yielding

$$\langle \eta(z') \eta(z'') \rangle = \langle \eta(z'')^2 \rangle \exp \left[-\frac{1}{3} \Delta \omega^2 \gamma (z' - z'') \right]. \quad (22)$$

As described in Appendix A, the term $\langle \eta(z'')^2 \rangle$ is given by:

$$\begin{aligned} \langle \eta(z'')^2 \rangle &= \eta(0)^2 \exp \left[-\gamma \Delta \omega^2 z'' \right] \\ &\quad + \frac{1}{3} \left[1 - \exp \left[-\gamma \Delta \omega^2 z'' \right] \right]. \end{aligned} \quad (23)$$

Plugging Eq. (23) into Eq. (22), yields

$$\begin{aligned} \langle \eta(z') \eta(z'') \rangle &= k_1 \exp \left[-\frac{k_2}{3} (z' + 2z'') \right] \\ &\quad + \frac{1}{3} \left[-\frac{k_2}{3} (z' - z'') \right] \quad \text{if } z' > z'', \end{aligned} \quad (24)$$

where

$$k_1 = \eta(0)^2 - \frac{1}{3}, \quad (25)$$

$$k_2 = \gamma \Delta \omega^2. \quad (26)$$

The same procedure can be repeated for $z' < z''$. The final expression for $\langle \eta(z') \eta(z'') \rangle$ is given by Eq. (27) in the bottom of this page. Plugging Eq. (27) back into Eq. (20), and solving the double integral yields Eq. (28) in the bottom of this page. Considering again Eq. (17), Eq. (18) and Eq. (28) yields the final result for the variance of G_{dB} , i.e.

$$\sigma_{dB}^2 = K^2 DOP_i^2 \left[I_2(L) - L_{pol}^2 \eta(0)^2 \right]. \quad (29)$$

Fig. 3 depicts Eq. (29) as a function of δ_{PMD} for three different configurations of input SOP (co-polarized, orthogonal and 45° polarized signals). It can be noticed that the variance of G_{dB}

$$\langle \eta(z') \eta(z'') \rangle = \begin{cases} k_1 \exp \left[-\frac{k_2}{3} (z' + 2z'') \right] + \frac{1}{3} \left[-\frac{k_2}{3} (z' - z'') \right] & \text{if } z' \geq z'', \\ k_1 \exp \left[-\frac{k_2}{3} (z'' + 2z') \right] + \frac{1}{3} \left[-\frac{k_2}{3} (z'' - z') \right] & \text{if } z' < z''. \end{cases} \quad (27)$$

$$\begin{aligned} I_2(L) &= 2 \left[\frac{k_1}{\alpha_i + \frac{2}{3}k_2} \cdot \frac{1 - \exp \left[-(\alpha_i + \frac{k_2}{3})L \right]}{\alpha_i + \frac{1}{3}k_2} - \frac{k_1}{\alpha_i + \frac{2}{3}k_2} \cdot \frac{1 - \exp \left[-(2\alpha_i + k_2)L \right]}{2\alpha_i + k_2} \right. \\ &\quad \left. + \frac{\frac{1}{3}}{\alpha_i - \frac{1}{3}k_2} \cdot \frac{1 - \exp \left[-(\alpha_i + \frac{1}{3}k_2)L \right]}{\alpha_i + \frac{k_2}{3}} - \frac{\frac{1}{3}}{\alpha_i - \frac{1}{3}k_2} \cdot \frac{1 - \exp \left[-2\alpha_i L \right]}{2\alpha_i} \right]. \end{aligned} \quad (28)$$

for the co-polarized and orthogonal configurations coincide. For low δ_{PMD} the variance of G_{dB} goes to zero. Such behavior is reasonable since in such case the input SOP of the optical fields are maintained during propagation, thus G_{dB} is completely deterministic. As δ_{PMD} increases, the two SOP do not maintain their relative orientation and σ_{dB}^2 increases, showing evidence of large fluctuations of G_{dB} . This is especially true for fiber lengths comparable with the PMD diffusion length [32]. As the decorrelation between the two signals increases, σ_{dB}^2 start decreasing, reaching a zero value for infinitely large δ_{PMD} . This is because for large δ_{PMD} the interaction of the two fields occurs over many correlation lengths in which the two fields orientation is random and uncorrelated. Therefore, under this condition, G_{dB} is the effective average of many independent realizations hence tends to a deterministic value because of the central limit theorem. In such conditions, the variance of the fluctuations of G_{dB} tends to zero.

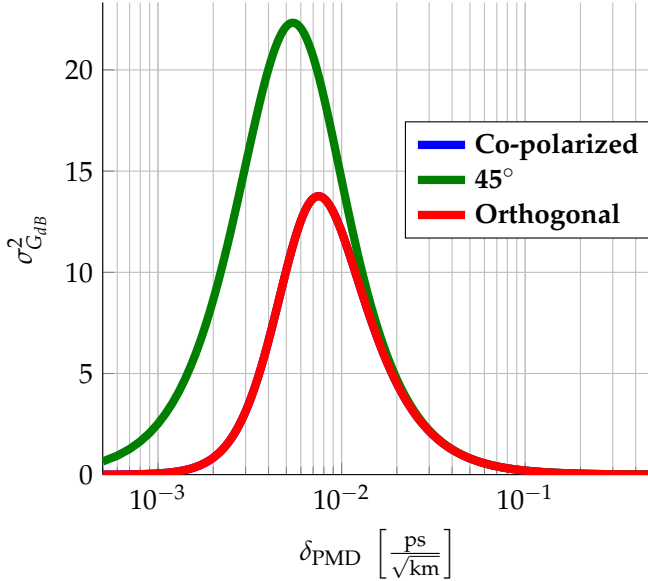


Figure 3. Variance of $G_{\text{dB}}(L)$ as a function of δ_{PMD} for a link length of 20 km, $K = 1$ dB/km, $\alpha_{i,\text{dB}} = 0.2$ dB/km and $\text{DOP}_i = 1$. Three different input SOP configurations are considered.

Considering both Fig. 2 and Fig. 3, it must be noticed that from a certain value of δ_{PMD} , the statistics of G_{dB} becomes independent from the input SOP configuration. This is true because under these conditions the SOP of the signal and the pump will be completely uncorrelated from their input states after few meters of propagations, therefore $G_{\text{dB}}(L)$ will not depend on the input SOP of the two optical fields.

C. Probability density function of $G_{\text{dB}}(L)$

In this Section we focus in deriving the probability density function (PDF) of the Raman gain $G_{\text{dB}}(L)$. While the results give in the previous two subsections on the mean and variance requires relatively standard probability theory mathematical background, the derivation of the PDF is much more involved and requires advanced mathematical tools. We start by observing that the only random component of $G_{\text{dB}}(L)$ given by

Eq. (3) is the stochastic integral

$$I = \int_0^z \eta(z') e^{-\alpha_i z'} dz'. \quad (30)$$

In order to compute the PDF of I we may apply the Markov property of the process $\eta(z)$ to efficiently obtain the PDF of I through matrix multiplication.

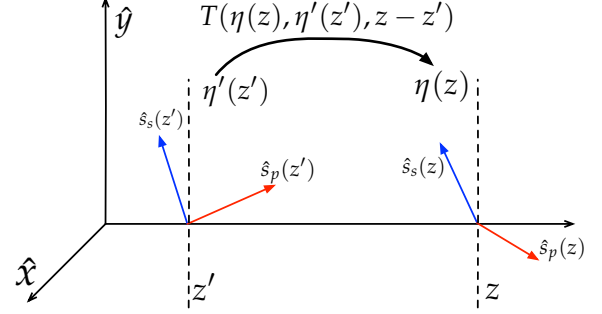


Figure 4. Qualitative description of Eq. (31). The two SOP of the involved optical signal evolve randomly from z' to z . Thanks to the Markov property, we can write the probability density function of η in z , by appropriately multiply the probability density function of η' in z' by the transition probability of the dot product of the two SOP from $\eta'(z')$ to $\eta(z)$.

As a first step, we will derive the equations that determine the evolution of the probability density function $P(\eta, z)$ of the random process $\eta(z)$. In particular, the following equations allows to evaluate $P(\eta, z)$ starting from $P(\eta', z')$, as schematically represented in Fig. 4, obtaining the following equation:

$$P(\eta, z) = \int T(\eta, \eta', z - z') P(\eta', z') d\eta', \quad (31)$$

whereas $T(\eta, \eta')$ is the transition probability of the dot product of the two SOP from $\eta'(z')$ to $\eta(z)$. We show appendix A that this transition probability is given by:

$$T(\eta, \eta', z) = \sum_{n=0}^{\infty} \exp \left[-\frac{\gamma}{6} n(n-1) \Delta \omega^2 z \right] L_n(\eta) L_n(\eta'), \quad (32)$$

where $L_n(\dots)$ are Legendre polynomials. Let us now consider $P(I, \eta, z)$, i.e. the joint probability of the variable η and of its integral I . Using the Markov property we obtain

$$P(I, \eta, z + dz) = \int T(\eta, \eta', dz) P[I - \eta' \exp(-\alpha_i z) dz, \eta', z] d\eta'. \quad (33)$$

If we now perform the following change of variable

$$\zeta = \frac{1 - \exp(-\alpha_i z)}{\alpha_i}, \quad (34)$$

$$z = -\frac{1}{\alpha_i} \ln(1 - \alpha_i \zeta), \quad (35)$$

into Eq. (33), we obtain

$$P(I, \eta, \zeta + d\zeta) = \int T \left(\eta, \eta', \frac{d\zeta}{1 - \alpha_i \zeta} \right) P(I - \eta' d\zeta, \eta', \zeta) d\eta'. \quad (36)$$

Integrating over a finite $\Delta\zeta$ we obtain

$$P(I, \eta, \zeta + \Delta\zeta) = \int T(\eta, \eta', \Delta z) P(I - \eta' \Delta\zeta, \eta', \zeta) d\eta', \quad (37)$$

where

$$\Delta z = -\frac{1}{\alpha_i} \log \left(\frac{1 - \alpha_i \zeta + \Delta\zeta}{1 - \alpha_i \zeta} \right). \quad (38)$$

Equation (37) can be solved iteratively from 0 to z , with initial condition

$$P(I, \eta, 0) = \delta(I) \delta(\eta - \eta_0). \quad (39)$$

Furthermore, to approximate the integral of Eq. (37) with a discrete sum over a grid, we integrate it over the interval

$$\begin{cases} [\eta_k - \frac{\Delta\eta}{2}, \eta_k + \frac{\Delta\eta}{2}], & \text{for } \eta_k \neq \pm 1, \\ [-1, -1 + \frac{\Delta\eta}{2}], & \text{for } \eta_k = -1, \\ [1 - \frac{\Delta\eta}{2}, 1], & \text{for } \eta_k = 1, \end{cases} \quad (40)$$

for the variable η , whereas for the variable I we integrate over

$$\left[I_h - \frac{\Delta I}{2}, I_h + \frac{\Delta I}{2} \right], \quad (41)$$

therefore we have

$$Q(y_h, \eta_k, \zeta + \Delta\zeta) = \int \overline{T}(\eta_k, \eta', \Delta z) d\eta' \int_{I_h - \frac{\Delta I}{2}}^{I_h + \frac{\Delta I}{2}} P(I - \eta' \Delta\zeta, \eta', \zeta) dI, \quad (42)$$

where

$$\overline{T}(\eta_k, \eta', \Delta z) = \int_{\eta_k - \frac{\Delta\eta}{2}}^{\eta_k + \frac{\Delta\eta}{2}} T(\eta, \eta', \Delta z) d\eta \quad (43)$$

is the transition probability inside the interval of amplitude $\Delta\eta$ centered on η_k , and

$$Q(I_h, \eta_k, \zeta) = \int_{I_h - \frac{\Delta I}{2}}^{I_h + \frac{\Delta I}{2}} dI \int_{\eta_k - \frac{\Delta\eta}{2}}^{\eta_k + \frac{\Delta\eta}{2}} P(I, \eta, \zeta) d\eta \quad (44)$$

is the probability that the point (η, I) lies within the area centered in (η_k, I_h) . Let us now start with the iterative procedure starting from $z = \zeta = 0$. Using the initial condition Eq. (39) at the right-hand side of Eq. (44), yields, at the first step, $Q(I_h, \eta_k, \Delta\zeta)$ exactly. If the value of the discretization step Δz is large enough, then we may assume that $P(I, \eta, z)$ depends weakly on I and η within the quantization area, hence we may approximate the integral over I of the right-hand side of Eq. (42), for $\eta \simeq \eta_k$ as

$$\int_{I_h - \frac{\Delta I}{2}}^{I_h + \frac{\Delta I}{2}} P(I, \eta', \zeta) dI \simeq \sum_m Q(I_h, \eta'_m, \zeta) \delta(\eta' - \eta'_m). \quad (45)$$

In other words, $P(I, \eta', \zeta)$ has been replaced with a sum of delta functions with center in the quantization areas that gives

the same probability over the quantization area. Thus, plugging Eq. (45) into Eq. (42), and integrating over η' yields

$$Q(y_h, \eta_k, \zeta + \Delta\zeta) = \sum_m \overline{T}(\eta_k, \eta'_m, \Delta z) Q(I_h - \eta'_m \Delta\zeta, \eta'_m, \zeta), \quad (46)$$

where, using the results of Appendix A,

$$\overline{T}(\eta, \eta', \Delta z) = \sum_{n=0}^{\infty} \left(\frac{2n+1}{2} \right) \overline{P_n(\eta)} P_n(\eta') \exp \left[-\frac{\gamma}{6} n(n+1) \Delta\omega^2 \Delta z \right], \quad (47)$$

with

$$\begin{aligned} \overline{P_n(\eta)} &= \int_{\eta - \frac{\Delta\eta}{2}}^{\eta + \frac{\Delta\eta}{2}} P_n(\eta') d\eta' \\ &= G_n \left(\eta + \frac{\Delta\eta}{2} \right) - G_n \left(\eta - \frac{\Delta\eta}{2} \right), \end{aligned} \quad (48)$$

and where $G_n(\eta)$ is defined in Eq. (92) of appendix A. Equation (46) can be iterated to reach the final point of propagation $z = L$. The normalization condition

$$\sum_{h,k} Q(I_h, \eta_k, \zeta) = 1 \quad (49)$$

is rigorously verified at every step of the iterative procedure. In order to obtain the PDF of G_{dB} , one can simply marginalize Eq. (46) at the end of the iterative procedure, and then scale and shift the result. In the implementation of the iterative procedure described above, particular attention should be placed in the choice of the discretization step Δz . In particular Δz should be chosen smaller than the diffusion length, or normalized length, of the fiber i.e. the length over which the η variable loses correlation. but not very small, because otherwise the transition probability $T(\eta, \eta', \Delta z)$ becomes very narrow in $\eta - \eta'$, and the number of grid points for a good accuracy increases, causing potential memory problems. For this reason this iterative procedure is not very efficient in two regimes: for very large or very small values of δ_{PMD} .

In the first case, the diffusion length becomes very small, and so it does Δz , causing a proportional increase in the integration steps to be performed over z . When the effective length of the fiber comprises a large number of correlation length, the stochastic integral Eq. (30) is the sum of a large number of independent contributions and therefore, because of the central limit theorem, its distribution is well approximated by a Gaussian. In this case, the distribution of G_{dB} is fully characterized by its mean and variance given by Eq. (13) and (29). This Gaussian approximation works well for large δ_{PMD} , or long link lengths, as it has also been shown experimentally [28]–[31], [33].

As for the very low PMD regime, the iterative procedure that we have described can be troublesome due to the fact that good accuracy would require very small Δz and a large number of integration steps. However in this regime, for co-polarized or orthogonal input SOP (i.e. $\eta_0 = \pm 1$ respectively), some approximations can be applied in order to efficiently compute the PDF of G_{dB} . If $\eta_0 \neq \pm 1$, or, more precisely, if the distance

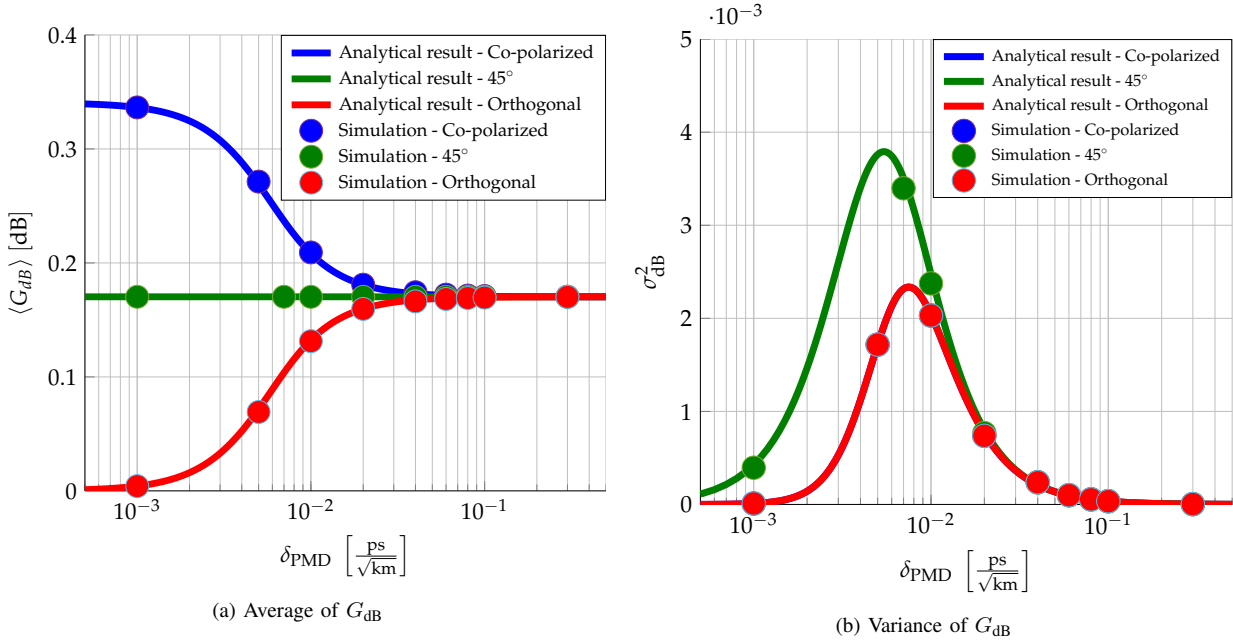


Figure 5. Comparison of theoretical and simulative results. Fiber length $L = 20$ km, $K = 1.3 \times 10^{-2}$ dB/km, $\Delta\lambda = 110$ nm, $C_r(\Delta\lambda) = 3 \times 10^{-4}$ 1/mW/km, $P_i = 10$ mW, $DOP_i = 1$, $\alpha_{i,dB} = 0.2$ dB/km. Eight different value of δ_{PMD} were considered. Three different input polarization configurations were considered: co-polarized optical fields $\eta_0 = 1$, 45° oriented optical fields $\eta_0 = 0$, orthogonally polarized optical fields $\eta_0 = -1$. Notice that the variance of G_{dB} for orthogonal and co-polarized input configurations completely overlaps.

between η_0 and ± 1 is significantly larger than half of the standard deviation of η , the statistics of G_{dB} is Gaussian and can be characterized by its mean and variance. Even though the low PMD regime may not be of significant practical interest, because in such case G_{dB} is practically deterministic, a detailed derivation of an analytic approximation of the PDF of G_{dB} in such scenario is described in details in appendix B.

III. COMPARISON WITH SIMULATIVE RESULTS

In order to verify and confirm the analytical results and their range of validity we have performed a Monte Carlo simulation campaign over a link under different PMD scenarios. In particular a fiber emulator based on the well-known coarse step method [35], [36], also known as waveplate model, was used. Such method approximates the continuous birefringence variations of a realistic fiber by the concatenation of fixed length birefringent plates, each of them characterized by a random orientation of its principal states of polarization (PSP) and a given differential group delay (DGD) that is determined by:

$$\Delta\tau_p = \sqrt{\frac{3\pi}{8}} \delta_{PMD} \sqrt{L_p}, \quad (50)$$

where L_p is the length of each section. L_p is chosen to be larger-equal than the correlation length of the fiber birefringence, that is typically of the order of few hundreds of meters.

In order to verify the correctness of the previous analytical results, we have considered 2 millions realization of $G_{dB}(L)$ obtained by the fiber emulator described above. The results are depicted in Fig. 5 for the mean and variance. The simulated results agree well with the theoretically calculated lines. The results shows that as δ_{PMD} increases the input configuration of the two SOP becomes completely irrelevant. The average

of G_{dB} becomes equal to the average G_{dB} for random input polarization [33]. The variance of G_{dB} goes instead to zero as δ_{PMD} is sufficiently large, and the PDF of G_{dB} becomes a Dirac delta. This is due to the fact that variations of G_{dB} are averaged out because the stochastic integral η is in this regime the sum of a large number of independent contributions.

In Fig. 6, a comparison between the simulated and theoretical PDF is depicted, for some intermediate PMD regimes, i.e. $\delta_{PMD} \leq 0.04$ ps/ \sqrt{km} that are those most common in modern SMF fibers. From the theoretical and simulative data, it is evident how for such PMD values of practical interest, the PDF of G_{dB} has a significant asymmetry around its mean, hence the Gaussian approximation proposed in [32], [33] is inadequate. Fig. 7 reports as an illustrative example the PDF of G_{dB} for a link length of $L = 20$ km and $\delta_{PMD} = 0.01$ ps/ \sqrt{km} : the PDF is clearly non Gaussian. This fact is even more evident for shorter link lengths ($L < 20$ km), due to the fact that the two optical fields maintain their relative polarization state for a significant fraction of the propagation, and therefore the input polarization configuration significantly affects the SRS induced gain or depletion. Such short link scenario is of extreme practical interest for PON, where the links are always shorter than 40 km. Fig. 6 shows good agreement between simulative and theoretically calculated results. In Fig. 6d, the approximation for the low PMD scenario developed in appendix B is used.

The excellent agreement shown in the previous figures between our analytical formulas and the extensive waveplate model simulations confirms the validity of our formalism and, from the other side, the accuracy of the waveplate model (that we will use again in the following section).

In the following section, we briefly discuss about a potential

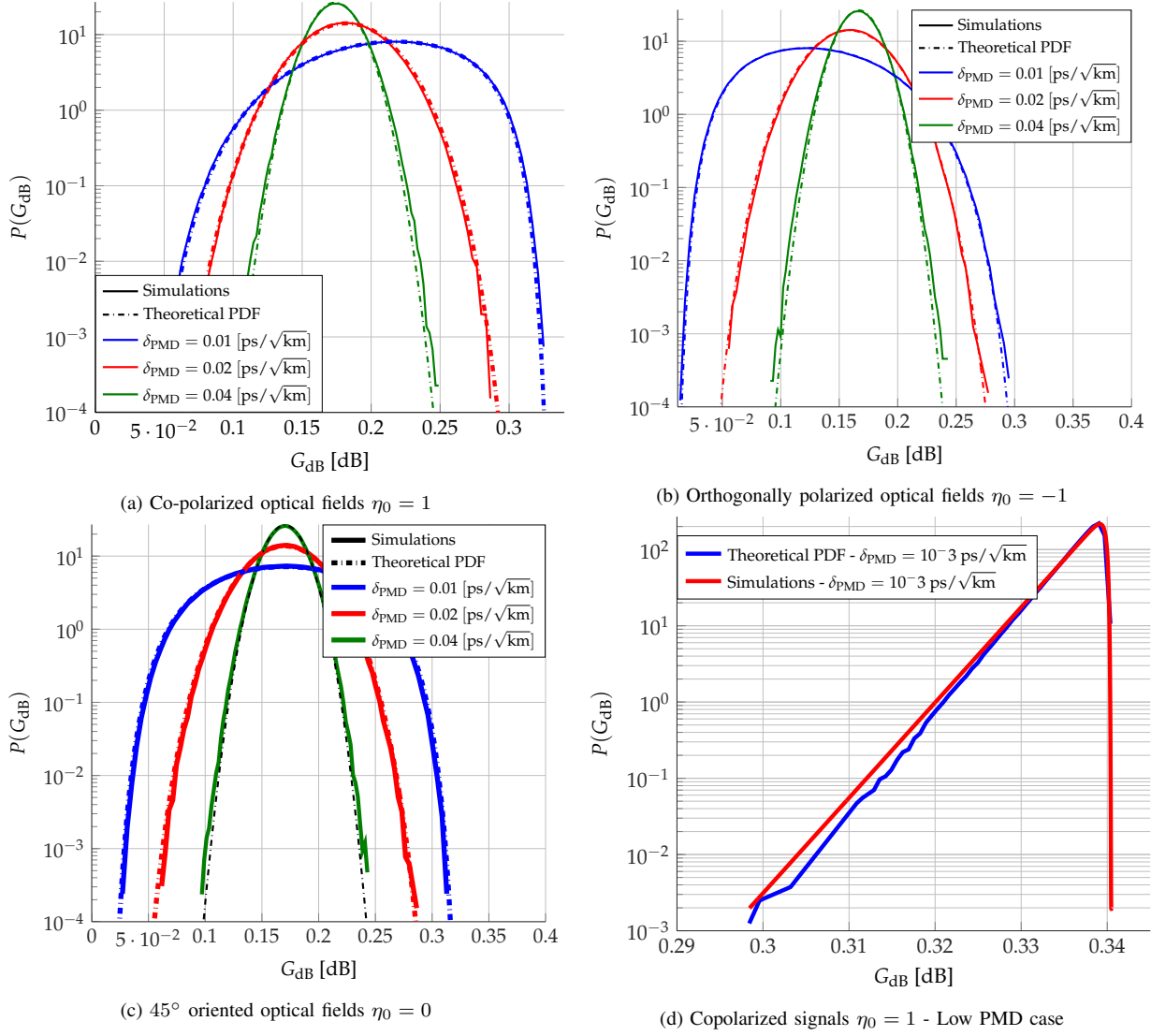


Figure 6. Comparison of theoretical and simulative PDF. Fiber length $L = 20$ km, $K = 1.3 \times 10^{-2}$ dB/km, $\Delta\lambda = 110$ nm, $C_r(\Delta\lambda) = 3 \times 10^{-4}$ 1/mW/km, $P_i = 10$ mW, $\text{DOP}_i = 1$, $\alpha_{i,dB} = 0.2$ dB/km. Three different value of δ_{PMD} were considered. Three different input polarization configurations were considered: co-polarized optical fields ($\eta_0 = 1$) Fig. 6a, orthogonally polarized optical fields ($\eta_0 = -1$) Fig. 6b, 45° oriented optical fields ($\eta_0 = 0$) Fig. 6c. In Fig. 6d the low pmd approximation developed in appendix B is used. Note that for the last case, we had to use a different scaling range on the x-axis compared to the previous three cases, since the resulting pdf is extremely compressed around its mean.

field of application of the analytical results previously developed.

IV. PON CASE STUDY AND APPLICATION

ITU-T has recently releases the new physical layer specification for the new standard for passive optical networks, titled NG-PON2 under Rec. G.989.2. Such standard introduces the new TWDM-PON (Time and Wavelength Division Multiplexed PON) high-performance transmission and considers N_{TWDM} , 100 GHz-spaced lambdas at 10 Gbit/s each in the L-band [42]. TWDM-PON is being designed in order to be fully compatible with the previous PON standards. However in full-coexistence scenarios, i.e. when the TWDM-PON will coexist on the same PON tree with previous standards (cfr. Fig. 8), namely GPON, XG-PON, and RF-Video, SRS may become detrimental. When the TWDM-PON power will be above a given threshold, lower wavelengths (e.g. GPON) channels will

act as Raman pumps for TWDM-PON channels: the former will undergo significant depletion, whereas the latter will be negligibly amplified.

In the last couple of years, the ongoing standardization process of NG-PON2 has required to study in details the effects of SRS in the full-coexistence scenario, in order to understand under what circumstances compatibility among different PON standards may exist. The works existing in literature [21], [24], [38] have always made use of simulations in order to take into account the stochastic nature of SRS. Such simulations are long and computational intensive, that may require several weeks of CPU time in order to produce reliable results. Thanks to the analytical results developed in this paper, such computational burden can be removed. To do so, however few consideration shall be made. All the results developed in section II refers to the SRS interaction between two optical signals, whereas in the previously described full coexistence

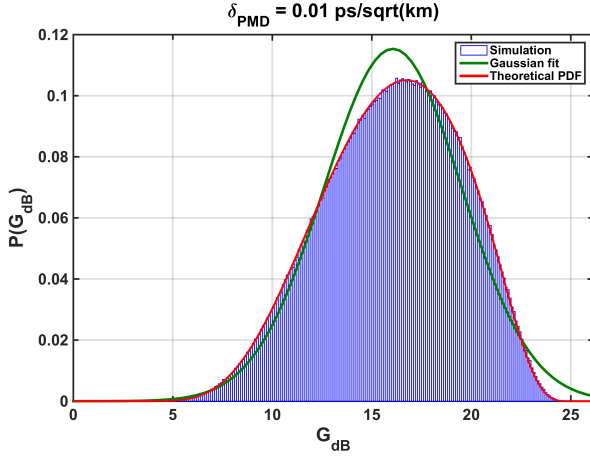


Figure 7. Simulated PDF of G_{dB} and relative Gaussian fitting. The data are relative to the following scenario: $L = 20$ km, $\eta_0 = 1$, $K = 1$ dB/km, $\Delta\lambda = 110$ nm, $\delta_{PMD} = 0.01$ ps/ $\sqrt{\text{km}}$, $\alpha_{i,dB} = 0.2$ dB/km. The inaccuracy of the Gaussian approximation is clear.

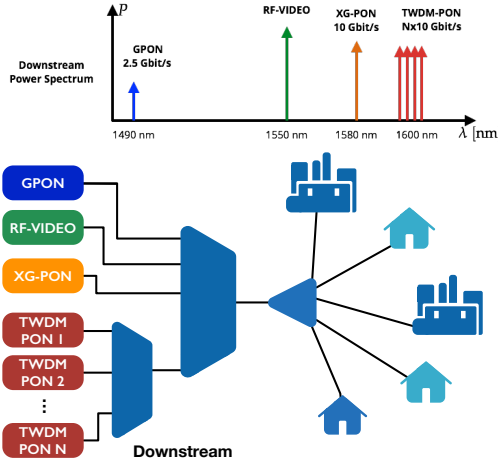


Figure 8. TWDM-PON full coexistence scenario. Downstream spectrum is depicted.

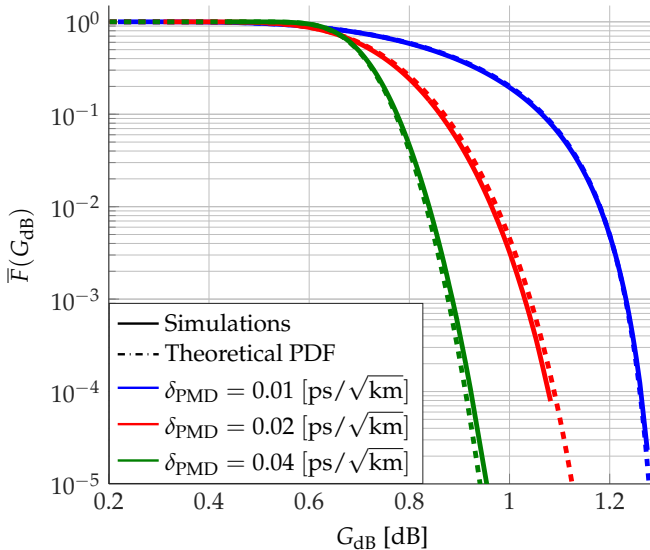


Figure 9. Comparison of empirical and theoretical survival functions of SRS induced depletion on GPON due to $N_{TWDM} = 4$ TWDM-PON channels with $P_{TWDM} = 10$ mW. $L = 20$ km, $\alpha_{dB} = 0.2$ dB/km. All TWDM-PON channels are co-polarized with respect to the GPON channel.

scenario such interaction is between more than two optical fields. For example the GPON channel may suffer some SRS induced depletion due to the presence of N_{TWDM} TWDM-PON channels. Under such circumstances, readily adapting Eq. (3), such depletion can be written as

$$G_{dB}(L) = 10 \log_{10}(e) C_r(\Delta\omega) P_{TWDM}(z=0) L_{eff,i} \left[1 + \sum_{n=1}^{N_{TWDM}} \int_0^L \eta_i(z) \exp(-\alpha z) dz \right], \quad (51)$$

where P_{TWDM} is the power of each TWDM-PON channel, and it is assumed to be constant across the TWDM-PON channel signal set. All TWDM-PON channels are also considered here to have the same DOP=1. $\Delta\omega$ is the spectral distance between the GPON and TWDM-PON channels, i.e. approximately 13 THz. The polarization averaged Raman gain coefficient can be assumed constant for all TWDM-PON signals, since it is almost flat on a scale of few hundreds of GHz.

In order to use our pump-probe analytical results also in such scenario, one can assume the N_{TWDM} channels to be a single equivalent channel with total power given by $N_{TWDM} P_{TWDM}$ and having a composite degree of polarization DOP_{comp} given by the normalized sum of all SOP of the TWDM-PON channels at the transmitter in $z = 0$. This assumption is legitimate since the TWDM-PON channels are only spaced 100 GHz one from the other, therefore during propagation, under standard PMD regimes and typical PON lengths (< 40 km), they will not decorrelate in polarization, and thus they will maintain the same DOP_{comp} (that was set at the transmitter) along the full fiber link. We will verify this assumption *a posteriori* by checking the obtained analytical result with an extensive waveplate simulation that on the contrary does not make any assumption on the evolution of the individual TWDM-PON channels.

This being said, Eq. (51), can be rewritten as

$$G_{dB}(L) = 10 \log_{10}(e) C_r(\Delta\omega) N_{TWDM} P_{TWDM} \left[L_{eff,i} + DOP_{comp} \int_0^L \eta(z) \exp(-\alpha z) dz \right]. \quad (52)$$

Equation (52) can then be evaluated using the previously discussed analytical results, in order to perform several system analysis about this scenario. Figure 9 depicts the comparison between the analytical survival function (sometimes also indicated in the literature as the complement of the cumulative distribution function) of Eq. (52) i.e.

$$\bar{F}(x) = Pr \{ G_{dB} > x \} \quad (53)$$

and the simulated survival function. The latter one has been obtained with the same Monte Carlo based fiber emulator described above. There is good agreement between the results, proving the validity of the previous assumptions.

A possible use of our theory is in the study of the probability that the SRS-induced depletion G_{dB} of a lower lambda channel (e.g. GPON) drops below a given system margin μ_{SRS} [38] and in the design of possible polarization launching strategies able

to reduce such probability [23], [24]. This outage probability is given by

$$P_{\text{OOS}} = \Pr \{G_{\text{dB}} \geq \mu_{\text{SRS}}\}. \quad (54)$$

Such outage probability can be evaluated numerically using Eq. (54), developing plot such as the one depicted in Fig. 9, thus avoiding the use of computationally expensive Monte Carlo simulations.

V. CONCLUSION

In this paper some novel theoretical results for the polarization related statistics of Raman crosstalk in single mode optical fiber are presented. In particular, closed formula for the average and variance of the Raman gain as function of the input states of polarization of the optical signals has been derived. In addition to this, a numerical method to exactly compute its probability density function has been explained. The obtained theoretical results show that the PDF of the Raman gain can be approximated as a Gaussian PDF, only for sufficiently long fibers. For fiber lengths shorter than 40 km, as frequently encountered in PON, the Gaussian approximation fails, whereas the theory presented in this paper maintains the same degree of accuracy of Monte Carlo simulations. The use of this theory may therefore be a valid alternative to computationally expensive Monte Carlo simulations to analyze PMD effect and Raman crosstalk interactions in PON. As an exemplary case, we have applied this theory to the study of propagation impairments caused by Raman crosstalk in a full-coexistence PON scenario, where a legacy GPON channel is randomly depleted by TWDM-PON channels. We believe that the results of this analysis, beside their obvious interest inside the standardization process for NG-PON2, can be useful in analyzing any optical communication systems where stimulated Raman scattering and polarization dispersion phenomena are simultaneously present.

APPENDIX A MOMENTS AND PDF OF $\eta(z)$

In this section we provide a detailed derivation of the moments and probability density function of $\eta(z)$, i.e. the dot product of the Stokes vector of two continuous wave optical fields separated by an angular frequency $\Delta\omega$ propagating through an optical fiber in the presence of polarization mode dispersion.

A. Moments

We start considering the law of infinitesimal rotation for birefringence [26], [27] in its Ito sense [43]

$$d\hat{s} = \omega d\vec{W}(z) \times \hat{s} - \frac{\gamma}{3}\omega^2 \hat{s} dz. \quad (55)$$

Such equation describes the evolution of a Stokes vector of an optical field at distance ω from the central frequency when travelling through a fiber affected by PMD. In particular γ is given by Eq. (11). $d\vec{W}(z)$ is the increment of a zero-mean, isotropic, three-dimensional Wiener process such that

$$d\vec{W}_i(z) \bullet d\vec{W}_j(z') = \gamma \delta(z - z') dz dz', \quad (56)$$

$$d\vec{W}_i(z) d\vec{W}_j(z') = \frac{\gamma}{3} \delta_{ij} \delta(z - z') dz dz', \quad (57)$$

where δ_{ij} is the Kronecker delta. We now consider the dot product of two Stokes vectors $\eta(z)$, defined by Eq. (5), placed at a spectral distance $\Delta\omega$ from one another. Using one of the two Stokes vector as reference, here indicated as \hat{s}_0 , the dot product $\eta(z)$ is equivalent to the projection of the unit Stokes vector \hat{s} onto a fixed direction of the Stokes space. Finding the statistics of $\eta(z)$ is equivalent to find the statistics of the x coordinate of a particle that is diffusing over the surface of a sphere. Using Eq. (55) and Eq. (56) one can write

$$d\eta = \Delta\omega d\vec{W} \bullet \hat{s}_{\Delta\omega} \times \hat{s}_0 - \frac{1}{3}\Delta\omega^2 \eta \gamma dz. \quad (58)$$

Differentiating using the rules of Ito calculus and Eq. (57) one gets

$$\begin{aligned} (d\eta)^2 &= \left(\Delta\omega d\vec{W} \bullet \hat{s}_{\Delta\omega} \times \hat{s}_0\right)^2 \\ &= \frac{\gamma}{3}\Delta\omega^2 dz |\hat{s}_{\Delta\omega} \times \hat{s}_0|^2 \\ &= \frac{\gamma}{3}\Delta\omega^2 (1 - \eta^2) dz. \end{aligned} \quad (59)$$

Using the Ito lemma

$$df(\eta) = \frac{df(\eta)}{d\eta} d\eta + \frac{1}{2} \frac{d^2 f(\eta)}{d\eta^2} (d\eta)^2, \quad (60)$$

one obtains

$$d\eta^n = n\eta^{n-1} d\eta + \frac{1}{2}n(n-1)\eta^{n-2}(d\eta)^2. \quad (61)$$

Plugging into this Eq. (58) and (59) and averaging with respect to the Wiener process yields a differential equation for the n -th order moment of η

$$\begin{aligned} d\langle\eta^n\rangle &= -\frac{1}{6}n(n+1)\langle\eta^n\rangle\Delta\omega^2\gamma dz \\ &\quad + \frac{1}{6}n(n-1)\langle\eta^{n-2}\rangle\Delta\omega^2\gamma dz, \end{aligned} \quad (62)$$

which can be solved iteratively from $n = 1$ using

$$\begin{aligned} \langle\eta^n(z)\rangle &= \eta^n(0) \exp\left[-\frac{1}{6}n(n+1)\Delta\omega^2\gamma z\right] \\ &\quad + \frac{1}{6}n(n-1)\Delta\omega^2\gamma \int_0^z \langle\eta^{n-2}(z')\rangle \\ &\quad \exp\left[-\frac{1}{6}n(n+1)\Delta\omega^2\gamma(z-z')\right] dz'. \end{aligned} \quad (63)$$

For $n = 1$ the average of $\eta(z)$ is obtained, i.e.

$$\langle\eta(z)\rangle = \eta(0) \exp\left[-\frac{1}{3}\Delta\omega^2\gamma z\right], \quad (64)$$

whereas the second order moment is given by

$$\begin{aligned} \langle\eta^2(z)\rangle &= \eta^2(0) \exp(-\Delta\omega^2\gamma z) \\ &\quad + \frac{1}{3}[1 - \exp(-\Delta\omega^2\gamma z)]. \end{aligned} \quad (65)$$

B. PDF of $\eta(z)$

In order to derive we probability density function of $\eta(z)$ we consider the generating function of $\eta(z)$, i.e. the Fourier transform of the PDF $P(\eta, z)$

$$\begin{aligned} G(\lambda, z) &= \left\langle \exp[-j\lambda\eta(z)] \right\rangle \\ &= \int_{-1}^1 P(\eta, z) \exp(-j\lambda\eta) d\eta. \end{aligned} \quad (66)$$

The previous equation can be differentiated using once again the rules of Ito calculus, yielding

$$dG = \left\langle -j\lambda G d\eta + \frac{1}{2}(-j\lambda)^2 G (d\eta)^2 \right\rangle. \quad (67)$$

Plugging in it Eq. (58) and (59) and removing the zero average terms one gets

$$\begin{aligned} dG &= \left\langle -j\lambda G \left(-\frac{1}{3}\Delta\omega^2\eta\gamma dz \right) \right. \\ &\quad \left. \frac{1}{2}(-j\lambda)^2 G \frac{\gamma}{3}\Delta\omega^2(1-\eta^2) dz \right\rangle. \end{aligned} \quad (68)$$

Using now the relationship $\langle \eta^n G \rangle = j^n \partial_\lambda^n G$ one gets

$$\partial_z G = -\frac{1}{3}\gamma\Delta\omega^2\lambda\partial_\lambda G - \frac{1}{6}\gamma\Delta\omega^2\lambda^2(G + \partial_\lambda^2 G). \quad (69)$$

From the previous partial differential equation one may derive the equation for the probability density function $P(\eta, z)$ by exploiting the well known properties of the Fourier transform, in particular

$$(\partial_\lambda^n) \mapsto (j\eta)^n, \quad (70)$$

$$\lambda^n \mapsto (j\partial_\eta)^n. \quad (71)$$

Using such relations one obtains

$$\begin{aligned} \frac{\partial P(\eta, z)}{\partial z} &= - \left[\frac{\partial}{\partial \eta} \left(-\frac{\gamma}{3}\Delta\omega^2\eta \right) P(\eta, z) \right] \\ &\quad + \frac{1}{2} \frac{\partial^2}{\partial \eta^2} \left\{ \left[\frac{\gamma}{3}\Delta\omega^2(1-\eta^2) \right] P(\eta, z) \right\}. \end{aligned} \quad (72)$$

This is the Fokker-Planck equation that describes the evolution of the probability density function of the dot product along the fiber. Eq. (72) has a non constant diffusion coefficient given by $D(\eta) = \frac{\gamma}{3}\Delta\omega^2(1-\eta^2) \geq 0$, and is defined for $-1 \leq \eta \leq +1$. Eq. (72) can be rearranged as

$$\frac{\partial P(\eta, z)}{\partial z} = \frac{\gamma}{6}\Delta\omega^2 \frac{\partial}{\partial \eta} \left[(1-\eta^2) \frac{\partial}{\partial \eta} P(\eta, z) \right]. \quad (73)$$

Solution of Eq. (72) is given by

$$P(\eta, z) = \sum_{n=0}^{\infty} c_n(z) L_n(\eta), \quad (74)$$

where $L_n(\eta)$ are the Legendre polynomials, solutions of the eigenfunction equation

$$\frac{\partial}{\partial \eta} \left[(1-\eta^2) \frac{\partial}{\partial \eta} L_n(\eta) \right] = -n(n+1) L_n(\eta). \quad (75)$$

$L_n(\eta)$ are the Legendre polynomials that can be defined by means of the Rodrigues formula [44], properly normalized

$$L_n(x) = \left(\frac{2n+1}{2} \right)^{1/2} \frac{1}{2^n n!} \frac{d^n}{dx^n} [(x^2-1)^n]. \quad (76)$$

The Legendre polynomials, with the considered normalization, are orthonormal in the interval of interest $[-1, 1]$ with respect to the L^2 inner product

$$\int_{-1}^{+1} L_m(x) L_n(x) dx = \delta_{mn}, \quad (77)$$

moreover they are a complete set in the same interval [45]

$$\sum_{n=0}^{\infty} L_n(x) L_n(x') = \delta(x-x'), \quad \text{for } x \in [-1, 1]. \quad (78)$$

Plugging Eq. (74) into Eq. (73), multiplying both sides by $L_m(\eta)$, integrating and using the orthonormality condition gives

$$\frac{dc_n}{dz} = -\frac{\gamma}{6} n(n+1) \Delta\omega^2 c_n, \quad (79)$$

thus the general solution of the Fokker-Planck equation (72) is given by

$$P(x_\omega, z) = \sum_{n=0}^{\infty} c_n(0) \exp \left[-\frac{\gamma}{6} n(n+1) \Delta\omega^2 z \right] L_n(\eta). \quad (80)$$

The initial coefficient $c_n(0)$ can be computed by the initial condition via

$$c_n(0) = \int_{-1}^1 P(\eta, 0) L_n(\eta) d\eta. \quad (81)$$

Being $L_0(\eta) = 1/\sqrt{2}$, the normalization of $P(\eta, 0)$ requires that $c_0(0) = 1/\sqrt{2}$ always. This condition, together with

$$\int_{-1}^1 L_0(x) L_n(x) dx = \frac{1}{\sqrt{2}} \int_{-1}^1 L_n(x) dx = 0, \quad \forall n \neq 0 \quad (82)$$

insures the normalization for all z of the probability density function, that is

$$\int_{-1}^1 P(\eta, z) d\eta = 1, \quad \forall z. \quad (83)$$

In the most interesting case of a deterministic initial condition with $\eta(z=0) = \eta_0$,

$$P(\eta, 0) = \delta(\eta - \eta_0), \quad (84)$$

the final result is obtained

$$P(\eta, z) = \sum_{n=0}^{\infty} \exp \left[-\frac{\gamma}{6} n(n+1) \Delta\omega^2 z \right] L_n(\eta_0) L_n(\eta). \quad (85)$$

For $\gamma\Delta\omega^2 z/3 \gg 1$, that correspond to the case of high PMD and fast decorrelation of the states of polarization of optical fields, the known result that η approaches a uniform distribution in the interval $[-1, 1]$ is obtained

$$P(\eta, z) \simeq \frac{1}{2}, \quad -1 \leq x \leq 1. \quad (86)$$

It can be noticed that Eq. (85) has an interesting reciprocity property. The transition probability from η_0 to η , is equal to the transition probability from η to η_0 .

For $z > 0$, the convergence of the series is ensured by the coefficient $c_n(z)$ dropping proportionally to a negative exponent of n^2 . For $z = 0$, the convergence to a delta function can be also numerically tested, although in general requires a large number of terms (larger than a hundred) to achieve a good accuracy. The vast majority of numerical computing software includes routines to efficiently compute Legendre polynomials, therefore Eq. (85) can be efficiently calculated. Furthermore the Legendre polynomials can be obtained by the recursive relation

$$P_0(x) = 1, \quad (87)$$

$$P_1(x) = x, \quad (88)$$

$$P_n(x) = \frac{2n-1}{n}xP_{n-1}(x) - \frac{n-1}{n}P_{n-2}(x), \quad (89)$$

followed by the normalization

$$L_n(x) = \sqrt{\frac{2n+1}{2}}P_n(x). \quad (90)$$

Finally a useful relation for the calculation of the cumulative distribution function of η is

$$P_n(x) = \frac{1}{2n+1} \frac{d}{dx} [P_{n+1}(x) - P_{n-1}(x)], \quad (91)$$

so that

$$\int_{-1}^{\eta} P_n(\eta') d\eta' = \frac{1}{2n+1} [P_{n+1}(\eta) - P_{n-1}(\eta)] = G_n(\eta), \quad (92)$$

from which the CDF of η can be easily evaluated. The analytic expression of $P(\eta, z)$, Eq. (85) may be useful in all cases where the mutual polarization of two initially copolarized optical fields at different frequency is of interest after propagation in a long optical fiber.

APPENDIX B PDF OF G_{dB} IN LOW PMD REGIME

In this section, an approximation to efficiently compute the PDF of G_{dB} for low values of δ_{PMD} and co-polarized or orthogonal input SOP ($\eta_0 = \pm 1$) will be proposed. During the following derivation we will consider $\eta_0 = 1$.

A. Lossless scenario

We start our analysis by considering the case $\alpha_i = 0$, that corresponds to no lossless propagation. It may be shown that in this case the variable I of Eq. (30) can be approximated to first order in $\Delta\omega^2\gamma z$ as

$$I = z - \frac{1}{2}\gamma\Delta\omega^2 \int_0^z [W_1(z')^2 + W_2(z')^2] dz', \quad (93)$$

where $W_1(z')$ and $W_2(z')$ are real and independent Wiener processes whose independent increments are characterized by $dW_i(z')dW_j(z'') = \frac{1}{3}dz'dz''\delta(z' - z'')$. The generating function of I is given by

$$G(\lambda, z) = \langle \exp(-j\lambda I) \rangle. \quad (94)$$

Even though its apparent simplicity thanks to the Gaussianity of $W_1(z')$ and $W_2(z')$, the calculation of $G(\lambda, z)$ is not trivial. A detailed derivation of it can be found in appendix D of [46]. The final result is

$$G(\lambda, z) = \exp(-j\lambda z) \text{sech} \left(\sqrt{-j\frac{1}{3}\lambda\gamma\Delta\omega^2 z^2} \right). \quad (95)$$

The PDF of I can be then computed numerically by considering the inverse fast Fourier transform of Eq. (95) or evaluated by truncation of an infinite series as shown in section B-B below.

B. Lossy Scenario

When considering a lossy scenario, i.e. $\alpha_i \neq 0$, it can be shown that in this case I can be approximated to first order in $\Delta\omega^2\gamma z$ as

$$I = L_{\text{eff},i} - \Delta I, \quad (96)$$

where $L_{\text{eff},i}$ is given by Eq. (4), and ΔI is given by

$$\Delta I = \frac{1}{2}\gamma\Delta\omega^2 \int_0^z \exp(-\alpha_i z') [W_1(z')^2 + W_2(z')^2] dz'. \quad (97)$$

If we define the auxiliary function

$$u(z) = \frac{1}{\alpha_i \sqrt{2[1 - (1 + \alpha_i z) \exp(-\alpha_i z)]}}, \quad (98)$$

such that

$$\frac{du}{dz} = \frac{z}{u} \exp(-\alpha_i z), \quad (99)$$

we can write the integral (97) as

$$\Delta I = \frac{1}{2}\gamma\Delta\omega^2 \int_0^z \frac{u'}{z'} [W_1(z')^2 + W_2(z')^2] du'. \quad (100)$$

Using the self-similarity property of the Wiener process [41], according to which two Wiener processes $W(z)$ and $W'(z)$ related by the identity

$$\sqrt{c}W'(z) = W(cz) \Rightarrow cW'(z) = W(cz)^2 \quad (101)$$

are equivalent processes, one can write

$$\Delta I = \frac{1}{2}\gamma\Delta\omega^2 \int_0^{u(z)} [W_1(u') + W_2(u')^2] du'. \quad (102)$$

It can be noticed that in Eq. (102), Eq. (97) has been reduced to the lossless case by using the scaled distance $u(z)$ of Eq. (98). The generating function is then

$$G(\lambda, z) = \text{sech} \left(\sqrt{j\frac{1}{3}\lambda\gamma\Delta\omega^2 u(z)^2} \right). \quad (103)$$

The PDF of ΔI is obtained by inverse Fourier transform of Eq. (103)

$$P(\Delta I) = \int \frac{1}{2\pi} \exp(j\lambda \Delta I) G(\lambda, z) d\lambda, \quad (104)$$

that can be computed numerically by means of fast Fourier transform algorithm, or evaluated by truncation of an infinite

series as shown in the next subsection. The SRS gain or depletion G_{dB} is thus given by

$$G_{dB} = K(L_{eff,i} + DOP_i I) \quad (105)$$

$$= K(L_{eff,i}(1 + DOP_i) - DOP_i \Delta I), \quad (106)$$

where K is a gain constant in dB/km and is given by $10 \log_{10}(e) C_r(\Delta\omega) P_i(z=0)$. The PDF of G_{dB} can thus be obtained by simple shift and scale of the PDF of ΔI .

As sanity check, it can be verified that the average gain obtained in the limit case of low δ_{PMD} is identical to the first order expansion with respect to γ of Eq. (13).

C. Inverse Laplace transform

As it has been highlighted in the previous paragraph, the probability density function of the SRS gain or depletion in the low PMD limit, can be computed by numerically inverse Fourier transforming the generating function of G_{dB} . In this section we give an expression of the PDF of G_{dB} as an infinite series, which once restricted to the first two terms gives an excellent analytic approximation of the PDF. We start transforming Eq. (103) in its Laplace transform equivalent

$$\begin{aligned} G(s, u(z)) &= \text{sech} \left(\sqrt{\frac{1}{3}} \gamma \Delta\omega^2 s u(z) \right) \\ &= \text{sech} (\varepsilon \sqrt{s} u(z)), \end{aligned} \quad (107)$$

where

$$\varepsilon = \sqrt{\frac{1}{3}} \gamma \Delta\omega^2. \quad (108)$$

Eq. (107) can be conveniently rewritten as a Laurent series, considering that its poles are given by

$$s_n = \frac{\pi^2}{4(\varepsilon u(z))^2} (1 + 2n)^2, \quad n = 0, 1, 2, \dots \quad (109)$$

and its residues

$$\kappa_n = \lim_{s \rightarrow s_n} \text{sech} (\varepsilon \sqrt{s} u(z)) = (-1)^n \frac{2\sqrt{s_n}}{\varepsilon u(z)} \quad (110)$$

$$= (-1)^n \frac{\pi(1 + 2n)}{(\varepsilon u(z))^2}. \quad (111)$$

The Laurent expansion of Eq. (107) can thus be written as

$$\begin{aligned} G(s, u(z)) &= \sum_{n=0}^{\infty} \kappa_n \frac{1}{s - s_n} \\ &= \sum_{n=0}^{\infty} (-1)^n \frac{\pi(1 + 2n)}{(\varepsilon u(z))^2} \frac{1}{s - \frac{\pi^2}{4(\varepsilon u(z))^2} (1 + 2n)^2}. \end{aligned} \quad (112)$$

Taking the inverse Laplace transform of the previous equation yields

$$\begin{aligned} P(\Delta I, u(z)) &= H(\Delta I) \sum_{n=0}^{\infty} (-1)^n \frac{\pi(1 + 2n)}{(\varepsilon u(z))^2} \\ &\quad \exp \left[-\frac{\pi^2}{4(\varepsilon u(z))^2} (1 + 2n)^2 \Delta I \right], \end{aligned} \quad (114)$$

where $H(\cdot)$ is the unit Heaviside step function. Equation (114) can thus be used with a finite n in order to obtain an

approximation of the PDF of G_{dB} in the low PMD scenario. In addition, the explicit analytic expression obtained retaining only the first two terms, corresponding to $n = 0$ and $n = 1$, is indistinguishable from the exact distribution for all values of ΔI (including at the position of the maximum of the distribution), with the exception of a very small region around $\Delta I = 0$.

REFERENCES

- [1] C. V. Raman, "A new radiation," *Indian Journal of physics*, vol. 2, pp. 387–398, 1928.
- [2] E. Woodbury and W. Ng, "Ruby laser operation in near ir," p. 2367, 1962.
- [3] R. H. Stolen, E. Ippen, and A. Tynes, "Raman oscillation in glass optical waveguide," *Applied Physics Letters*, vol. 20, no. 2, pp. 62–64, 1972.
- [4] R. H. Stolen and E. P. Ippen, "Raman gain in glass optical waveguides," *Applied Physics Letters*, vol. 22, no. 6, pp. 276–278, 1973. [Online]. Available: <http://scitation.aip.org/content/aip/journal/apl/22/6/10.1063/1.1654637>
- [5] J. AuYeung and A. Yariv, "Spontaneous and stimulated Raman scattering in long low loss fibers," *Quantum Electronics, IEEE Journal of*, vol. 14, no. 5, pp. 347–352, May 1978.
- [6] M. Ikeda, "Stimulated Raman amplification characteristics in long span single-mode silica fibers," *Optics Communications*, vol. 39, no. 3, pp. 148 – 152, 1981. [Online]. Available: <http://www.sciencedirect.com/science/article/pii/0030401881900444>
- [7] G. A. Koepf, D. M. Kalen, and K. H. Greene, "Raman amplification at 1.118 μm in single-mode fibre and its limitation by Brillouin scattering," *Electronics Letters*, vol. 18, pp. 942–943(1), October 1982.
- [8] Y. Aoki, S. Kishida, H. Honmou, K. Washio, and M. Sugimoto, "Efficient backward and forward pumping CW Raman amplification for InGaAsP laser light in silica fibres," *Electronics Letters*, vol. 19, pp. 620–622(2), August 1983.
- [9] E. Desurvire, M. Papuchon, J. Pocholle, J. Raffy, and D. Ostrowsky, "High-gain optical amplification of laser diode signal by Raman scattering in single-mode fibres," *Electronics Letters*, vol. 19, no. 19, pp. 751–753, September 1983.
- [10] J. Hegarty, N. Olsson, and L. Goldner, "CW pumped Raman preamplifier in a 45 km-long fibre transmission system operating at 1.5 μm and 1 Gbit/s," *Electronics Letters*, vol. 21, no. 7, pp. 290–292, March 1985.
- [11] H. Kidorf, K. Rottwitt, M. Nissov, M. Ma, and E. Rabarjaona, "Pump interactions in a 100-nm bandwidth raman amplifier," *Photonics Technology Letters, IEEE*, vol. 11, no. 5, pp. 530–532, May 1999.
- [12] S. Namiki and Y. Emori, "Ultrabroad-band raman amplifiers pumped and gain-equalized by wavelength-division-multiplexed high-power laser diodes," *Selected Topics in Quantum Electronics, IEEE Journal of*, vol. 7, no. 1, pp. 3–16, Jan 2001.
- [13] M. Islam, "Raman amplifiers for telecommunications," *Selected Topics in Quantum Electronics, IEEE Journal of*, vol. 8, no. 3, pp. 548–559, May 2002.
- [14] J. Bromage, "Raman amplification for fiber communications systems," *Lightwave Technology, Journal of*, vol. 22, no. 1, pp. 79–93, Jan 2004.
- [15] B. Zhu, X. Liu, S. Chandrasekhar, D. Peckham, and R. Lingle, "Ultra-Long-Haul Transmission of 1.2-Tb/s Multicarrier No-Guard-Interval CO-OFDM Superchannel Using Ultra-Large-Area Fiber," *Photonics Technology Letters, IEEE*, vol. 22, no. 11, pp. 826–828, June 2010.
- [16] G. Charlet, J. Renaudier, and M. Salsi, "Ultra high capacity transmission over transoceanic distances," in *Optical Communication (ECOC), 2014 European Conference on*, Sept 2014, pp. 1–3.
- [17] J. Cai, Y. Sun, H. Zhang, H. Batshon, M. Mazurczyk, O. Sinkin, D. Foursa, and A. Pilipetskii, "49.3 Tb/s Transmission Over 9100 km Using C+L EDFA and 54 Tb/s Transmission Over 9150 km Using Hybrid-Raman EDFA," *Lightwave Technology, Journal of*, vol. 33, no. 13, pp. 2724–2734, July 2015.
- [18] M. Phillips and D. Ott, "Crosstalk due to optical fiber nonlinearities in WDM CATV lightwave systems," *Lightwave Technology, Journal of*, vol. 17, no. 10, pp. 1782–1792, Oct 1999.
- [19] F. Coppinger, L. Chen, and D. Piehler, "Nonlinear Raman cross-talk in a video overlay passive optical network," in *Optical Fiber Communications Conference, 2003. OFC 2003*, March 2003, pp. 285–286 vol.1.
- [20] M. Aviles, K. Litvin, J. Wang, B. Colella, F. Effenberger, and F. Tian, "Raman crosstalk in video overlay passive optical networks," in *Optical Fiber Communication Conference, 2004. OFC 2004*, vol. 2, Feb 2004, pp. 3 pp. vol.2–.

- [21] R. Gaudino, V. Curri, and S. Capriata, "Propagation impairments due to Raman effect on the coexistence of GPON, XG-PON, RF-video and TWDM-PON," in *Optical Communication (ECOC 2013)*, 39th European Conference and Exhibition on, Sept 2013, pp. 1–3.
- [22] ITU-T, "40-Gigabit capable passive optical networks (NG-PON2)," *Recommendation G.989.1*.
- [23] M. Cantono, V. Curri, A. Mecozzi, and R. Gaudino, "Interplay between Raman and polarization effects in next-generation passive optical networks," *Opt. Express*, vol. 23, no. 11, pp. 13 924–13 936, Jun 2015. [Online]. Available: <http://www.opticsexpress.org/abstract.cfm?URI=oe-23-11-13924>
- [24] M. Cantono, A. Mecozzi, V. Curri, and R. Gaudino, "Optimal Polarization Launch for Raman Depletion Minimization in GPON and TWDM-PON Coexistence," in *Optical Fiber Communication Conference*. Optical Society of America, 2015.
- [25] R. H. Stolen, "Polarization effects in fiber Raman and Brillouin lasers," *Quantum Electronics, IEEE Journal of*, vol. 15, no. 10, pp. 1157–1160, Oct 1979.
- [26] G. Foschini and C. Poole, "Statistical theory of polarization dispersion in single mode fibers," *Lightwave Technology, Journal of*, vol. 9, no. 11, pp. 1439–1456, Nov 1991.
- [27] J. Gordon and H. Kogelnik, "Pmd fundamentals: Polarization mode dispersion in optical fibers," *Proceedings of the National Academy of Sciences*, vol. 97, no. 9, pp. 4541–4550, 2000.
- [28] D. Mahgerefteh, H.-Y. Yu, D. Butler, J. Goldhar, D. Wang, E. Golovchenko, A. Pilipetskii, C. Menyuk, and L. Joneckis, "Effect of randomly varying birefringence on the Raman gain in optical fibers," in *Lasers and Electro-Optics, 1997. CLEO '97., Summaries of Papers Presented at the Conference on*, vol. 11, May 1997, pp. 447–447.
- [29] A. Berntson, S. Popov, E. Vanin, G. Jacobsen, and J. Karlsson, "Polarisation dependence and gain tilt of Raman amplifiers for WDM systems," in *Optical Fiber Communication Conference and Exhibit, 2001. OFC 2001*, vol. 1, March 2001, pp. MI2_1–MI2_3 vol.1.
- [30] P. Ebrahimi, M. Hauer, Q. Yu, R. Khosravani, D. Gurkan, D. Kim, D. Lee, and A. Willner, "Statistics of polarization dependant gain in Raman fiber amplifiers due to PMD," in *Lasers and Electro-Optics, 2001. CLEO '01. Technical Digest. Summaries of papers presented at the Conference on*, May 2001, pp. 143–144.
- [31] H. Kee, C. Fludger, and V. Handerek, "Statistical properties of polarisation dependent gain in fibre Raman amplifiers," in *Optical Fiber Communication Conference and Exhibit, 2002. OFC 2002*, Mar 2002, pp. 180–181.
- [32] Q. Lin and G. P. Agrawal, "Vector theory of stimulated Raman scattering and its application to fiber-based Raman amplifiers," *J. Opt. Soc. Am. B*, vol. 20, no. 8, pp. 1616–1631, Aug 2003. [Online]. Available: <http://josab.osa.org/abstract.cfm?URI=josab-20-8-1616>
- [33] E. S. Son, J. Lee, and Y. Chung, "Statistics of polarization-dependent gain in fiber Raman amplifiers," *Lightwave Technology, Journal of*, vol. 23, no. 3, pp. 1219–1226, March 2005.
- [34] G. Foschini and G. Vannucci, "Characterizing filtered light waves corrupted by phase noise," *Information Theory, IEEE Transactions on*, vol. 34, no. 6, pp. 1437–1448, Nov 1988.
- [35] C. Poole and D. Favin, "Polarization-mode dispersion measurements based on transmission spectra through a polarizer," *Lightwave Technology, Journal of*, vol. 12, no. 6, pp. 917–929, Jun 1994.
- [36] D. Marcuse, C. Menyuk, and P. Wai, "Application of the Manakov-PMD equation to studies of signal propagation in optical fibers with randomly varying birefringence," *Lightwave Technology, Journal of*, vol. 15, no. 9, pp. 1735–1746, Sep 1997.
- [37] C. Fludger, V. Handerek, and R. Mears, "Pump to signal RIN transfer in Raman fiber amplifiers," *Lightwave Technology, Journal of*, vol. 19, no. 8, pp. 1140–1148, Aug 2001.
- [38] V. Curri, S. Capriata, and R. Gaudino, "Outage probability due to Stimulated Raman Scattering in GPON and TWDM-PON coexistence," in *Optical Fiber Communication Conference*. Optical Society of America, 2014, p. M31.2. [Online]. Available: <http://www.opticsinfobase.org/abstract.cfm?URI=OFC-2014-M31.2>
- [39] E. DiBenedetto, *Real Analysis*. Birkhäuser Boston, 2002.
- [40] A. Mecozzi and M. Shtaif, "Study of the two-frequency moment generating function of the PMD vector," *Photonics Technology Letters, IEEE*, vol. 15, no. 12, pp. 1713–1715, 2003.
- [41] A. Papoulis and S. Pillai, *Probability, Random Variables, and Stochastic Processes*. McGraw-Hill, 2002.
- [42] Y. Luo, X. Zhou, F. Effenberger, X. Yan, G. Peng, Y. Qian, and Y. Ma, "Time - and Wavelength-Division Multiplexed Passive Optical Network (TWDM-PON) for Next-Generation PON Stage 2 (NG-PON2)," *Lightwave Technology, Journal of*, vol. 31, no. 4, pp. 587–593, Feb 2013.
- [43] C. Gardiner, *Handbook of Stochastic Methods for Physics, Chemistry, and the Natural Sciences*, ser. Springer complexity. Springer, 2004.
- [44] K. Tang, *Mathematical Methods for Engineers and Scientists 3: Fourier Analysis, Partial Differential Equations and Variational Methods*. Springer, 2006.
- [45] W. Kaplan, *Advanced Calculus*. Addison-Wesley, 2003.
- [46] A. Mecozzi and M. Shtaif, "Signal-to-noise-ratio degradation caused by polarization-dependent loss and the effect of dynamic gain equalization," *Lightwave Technology, Journal of*, vol. 22, no. 8, pp. 1856–1871, Aug 2004.